PAPER

DUV fluorescence bioimaging study of the interaction of partially reduced graphene oxide and liver cancer cells

To cite this article: Radovan Dojilovi *et al* 2018 *2D Mater.* **5** 045019

2D Materials

PAPER

RECEIVED
22 April 2018

REVISED
15 July 2018

ACCEPTED FOR PUBLICATION
31 July 2018

PUBLISHED
13 August 2018

DUV fluorescence bioimaging study of the interaction of partially reduced graphene oxide and liver cancer cells

Radovan Dojčilović[1,2], Jelena D Pajović[3,4], Dušan K Božanić[1,5], Nataša Jović[1], Vera P Pavlović[6], Vladimir B Pavlović[7,8], Lea Lenhardt Acković[1], Ivana Zeković[1], Miroslav Dramićanin[1], Slavka Kaščaková[9,10], Matthieu Réfrégiers[4], Goran Rašić[11,12], Branislav Vlahović[11,12,13] and Vladimir Djoković[1,13]

[1] Vinča Institute of Nuclear Sciences, University of Belgrade, PO Box 522, 11001 Belgrade, Serbia
[2] Department of Chemistry and Biochemistry, University of Notre Dame, 251 Nieuwland Science Hall, Notre Dame, IN 46556, United States of America
[3] Faculty of Physics, University of Belgrade, PO Box 368, 11001 Belgrade, Serbia
[4] DISCO beamline, Synchrotron SOLEIL, F-91192 Gif sur Yvette, France
[5] DESIRS beamline, Synchrotron SOLEIL, F-91192 Gif sur Yvette, France
[6] Faculty of Mechanical Engineering, University of Belgrade, 11000 Belgrade, Serbia
[7] Faculty of Agriculture, University of Belgrade, 11000 Belgrade, Serbia
[8] Institute of Technical Sciences, Serbian Academy of Sciences and Arts, Belgrade, Serbia
[9] Inserm Unité 1193, F-94800 Villejuif, France
[10] Univ. Paris-Sud XI, UMR-S1193, F-94800 Villejuif, France
[11] North Carolina Central University, Durham, NC, United States of America
[12] NASA University Research Center for Aerospace Device Research and Education and NSF Center of Research Excellence in Science and Technology Computational Center for Fundamental and Applied Science and Education, Durham, NC, United States of America
[13] Authors to whom any correspondence should be addressed.

E-mail: vlahovic@nccu.edu **and** djokovic@vin.bg.ac.rs

Keywords: bioimaging, graphene oxide, fluorescence, cancer, cells

Supplementary material for this article is available online

Abstract

The interaction of partially reduced graphene oxide (prGO) and Huh7.5.1 liver cancer cells was investigated by means of DUV fluorescence bioimaging. The prGO sample was obtained by the reduction (to a certain extent) of the initially prepared graphene oxide (GO) nanosheets with hydrazine. The fluorescence of the GO nanosheets increases with time of the reduction due to a change in ratio of the sp^2 and sp^3 carbon sites and the prGO sample was extracted from the dispersion after 6 min, when the intensity of the fluorescence reached its maximum. The reduction process was left to proceed further to saturation until highly reduced graphene oxide (denoted here as rGO) was obtained. GO, prGO and rGO samples were investigated by structural (scanning electron microscopy (SEM), scanning transmission electron microscopy coupled with energy dispersive spectrometry (STEM-EDS)) and spectroscopic (UV–vis, photoluminescence (PL), Raman) methods. After that, Huh7.5.1 cells were incubated with GO, prGO and rGO nanosheets and used in bioimaging studies, which were performed on DISCO beamline of synchrotron SOLEIL. It was found that the prGO significantly enhanced the fluorescence of the cells and increased the intensity of the signal by ~2.5 times. Time-lapse fluorescence microscopy experiments showed that fluorescence dynamics strongly depends on the type of nanosheets used. The obtained prGO nanostructure can be easily conjugated with aromatic ring containing drugs, which opens a possibility for its applications in fluorescence microscopy monitored drug delivery.

1. Introduction

Graphene-based nanomaterials recently emerged as novel carriers in drug delivery applications [1, 2]. Graphene oxide (GO) and reduced GO (rGO) display advantageous characteristics as biosensing platforms due to the high surface area, excellent biocompatibility and ability to interact with proteins and polysaccharides [3–5]. GO exhibits wide fluorescence emission (280–500 nm) [6] that can be used to track the transport of the graphene-based nanocarriers to the particular cells by means of fluorescent microscopy

[7]. In fluorescent bioimaging, it is also important to use hydrophilic probes with well-defined sizes and specific optical properties. It was shown that the optical properties of GO could be controlled by changing its surface chemistry [8–10]. GO is an electronically hybrid material that possesses both conducting π-states from sp^2 carbon sites and a large energy gap between the σ-states of its sp^3-bonded carbons. The control of the ratio of the sp^2 and sp^3 fractions by the reduction process enables one to tune its bandgap and, therefore, to controllably transform GO from an insulator to a graphene-like semi-conductor [11]. With the partial reduction of GO, it is possible to influence the size of sp^2 clusters, which affects the fluorescence emission and enhances the quantum yield [8]. In the present study, we decided to investigate the interaction of this intermediate form, partially reduced graphene oxide (prGO), with cancer liver cells (Huh7.5.1 cell line) by using DUV fluorescence microscopy. We believe that the pronounced fluorescence of prGO will enable its easier detection in the certain cell compartments, which is very important if these nanostructures are going to be used in drug delivery applications.

The interaction of graphene-based nanosheets with live cells may induce significant changes in the functioning of the cells and distinct toxic effects. Previous optical microscopy studies revealed that GO and rGO are internalized in cells in a different way, while their toxicity is highly dependent on the presence of the surface oxygen groups [12, 13]. The changes in the metabolism may be followed by observing the changes in the autofluorescence of the cells, since autofluorescent species, particularly aromatic amino acids and NADH, are involved in mitochondrial function, energy metabolism, calcium homeostasis, gene expression, oxidative stress, aging and apoptosis [14, 15]. The study is focused on the fluorescence properties of the cancer Huh7.5.1 cells after their interaction with GO, prGO and rGO sheets. We also followed the changes in fluorescence dynamics of these GO-based species when they are in contact with the cells.

2. Materials and methods

2.1. GO and the reduced GO

GO was synthesized by using modified Hummers method according to the procedure found in [16]. A 150 g of expanded graphite (EG) was used as a starting material, while sulphuric acid (95%–98% H_2SO_4, Sigma Aldrich) was used as the intercalating compound. Sulphuric acid (6 ml) was added to the pilled pieces of EG and mixed at 0 °C for 2 h. The mixture was left overnight and kept at room temperature. Oxidation was carried out by adding 450 mg of potassium permanganate ($KMnO_4$). After adding 28 ml of DI water, the mixture was kept in oil bath at 90 °C–95 °C for 2 h. Then, the oxidized graphite mixture was cooled down to the room temperature. A possible reduction of the product was stopped by adding 84 ml of 3% solution of H_2O_2. Several cycles of centrifugation (at 5500 rpm) and washing with 5% HCl solution were conducted until brown solution of graphite oxide (GtO) was obtained. The sonication of GtO solution with Branson W-450 D Digital Sonifier with 20% amplitude (80 W) for 10 min resulted in a change of colour from light brown to light yellow. Transparent light yellow supernatants of GO were obtained after another cycle of centrifugation and washing.

The reduction of the obtained GO was carried out by using 30% solution of hydrazine hydrate (N_2H_4, Sigma Aldrich). First, the beaker with 0.1 mg ml^{-1} of GO solution was heated in oil bath at 95 °C. After that, 100 μl of hydrazine solution was added into heated GO solution to initiate the reduction process. At certain time intervals during the reduction, equal amounts of GO were extracted and diluted with DI water in order to stop the process. The partially reduced GO samples extracted at different reduction times were stable for more than a month after the preparation. The reduced GO sample was obtained at the end of the preparation procedure (after 45 min of reduction). It was less stable; the sheets tended to agglomerate after few days. This sample was studied immediately after its preparation.

2.2. Methods

The morphology of GO was investigated by using a JEOL JSM-6390 scanning electron microscope (SEM). Because of the low electrical conductivity of GO, the surface was covered with thin layer of gold. The micrographs of GO were obtained at operating voltage of 13 kV.

The structure and morphology of the GO, prGO and rGO samples were investigated by probe aberration corrected scanning transmission electron microscope (STEM) (FEI Titan 80-300) coupled with a SuperX energy dispersive spectrometer (SuperX EDS) with the four silicon drift detectors (SDD) (Bruker). Aqueous dispersions of the GO, prGO and rGO were deposited on carbon coated copper grids using an automatic pipette. The samples were left to dry under ambient conditions before they were transferred to the microscope chamber.

A fully automated Raman microscope (LabRAM HR Evolution) was used for Raman spectroscopy measurements. The spectra were obtained over the Raman shift range from 1000 to 2000 cm^{-1} using acquisition time of 10 s. The samples were excited by 532 nm laser light (with 1.08 mW of incident power) and the data were collected by using a 50 × objective.

The UV–vis absorption measurements of the aqueous dispersions were carried out on a Thermo Evolution 600 spectrophotometer.

The photoluminescence (PL) spectra of aqueous dispersions of GO, prGO and rGO were recorded using a PerkinElmer LS45 fluorescence spectrophotometer. Fluorescence excitation emission matrices were

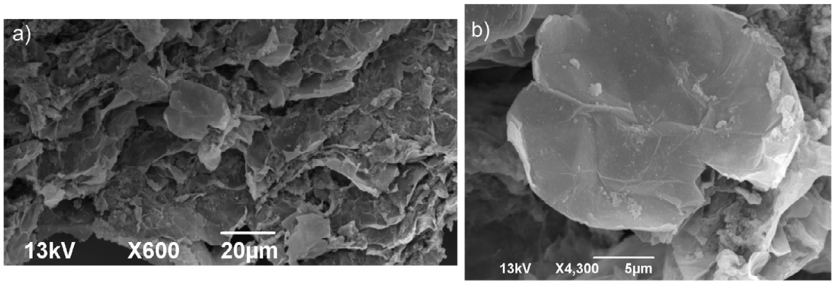

Figure 1. (a) Scanning electron microscopy (SEM) micrograph of the obtained GO sheets. (b) Selected GO sheet at higher magnification.

recorded on a Fluorolog-3 spectrofluorometer system (Model FL3-221, Horiba Jobin Yvon). Xenon lamp (450 W) was used as an excitation source. Both excitation and emission monochromators were double grating, with dispersion of 2.1 nm mm^{-1} (1200 grooves nm^{-1}). All measurements were performed in the front face geometry at room temperature. To obtain the fluorescence excitation emission matrices, the emission spectra were recorded in the range from 330 to 650 nm at 2 nm steps and in the excitations range from 270 to 430 nm at 2.5 nm steps. For these measurements, excitation slit was set at 6 nm, emission slit was at 2 nm and integration time was fixed to 0.4 ms. Variations of the excitation power were corrected using reference photodetector.

2.3. Cell line and the preparation of biological samples

Human hepatocellular carcinoma-derived Huh7.5.1 cells were routinely cultured as monolayer and were grown in Dulbecco's modified Eagle's medium (DMEM) supplemented with 10% fetal calf serum, penicillin and streptomycin. The cells were maintained at 37 °C in a humidified atmosphere of 5% CO_2.

For DUV fluorescence imaging studies, the Huh7.5.1 cells were plated in plastic Petri dishes containing 25 mm round quartz coverslip and incubated for 24 h. Cell attachment was monitored by visible inspection using a microscope. Thereafter, cells were incubated with GO, prGO and rGO sheets for 5 h. The cell's culture medium (3 ml) was mixed with 300 μl of the GO, prGO and rGO dispersions (30 $\mu g\,ml^{-1}$). After the incubation, the cells were washed with PBS, fixed with 4% of PFA, rinsed in distilled water and air dried before being used for bioimaging. The control sample was prepared in the same way but without adding GO, prGO or rGO.

2.4. Deep-UV fluorescence microscopy

The fluorescence images of Huh7.5.1 cells and Huh7.5.1 cells incubated with GO, prGO and rGO were acquired on TELEMOS endstation of DISCO beamline (SOLEIL synchrotron facility, France). Synchrotron light source was monochromatized to provide an excitation wavelength of 270 nm and the flux of the beam was less than $7 \cdot 10^{10}$ photons s^{-1}. DISCO beamline is optimized for the investigations of the biological samples and the intensity of the beam was adjusted to minimize the possibility of damaging the cells. The fluorescence of the control and incubated cells was collected in the [327–353 nm], [370–410 nm] and [420–480 nm] wavelength ranges for 30 s. To ensure consistency of the observations at least 30 different locations (80×80 μm) were investigated. An ultrafluar 100 × glycerin immersion objective (Zeiss, Germany) and PIXIS 1024-BUV EM-CCD camera (Princeton, USA) were used for recording images. Time-lapse experiments were performed to study the fluorescence dynamics of the control and incubated cells. The evolution of the fluorescence signal was followed by recording the fluorescent image every 2 min for 30 s. FIJI software [17] was employed in order to analyse the obtained fluorescence images. The normalization of original intensities I was performed by using following formula:

$$f(t_i) = \frac{I(t_i) - I_{min}}{I_{max} - I_{min}}, \qquad (1)$$

where $f(t_i)$ are the normalized intensities with respect to the minimum (I_{min}) and maximum (I_{max}) values of the $\{I(t_i)\}$ set.

3. Results and discussion

3.1. Structure and optical properties of GO, prGO and rGO

Modified Hummers method was used for the fabrication of GO and figure 1 shows the SEM micrograph of the obtained GO sample. The SEM image of a selected exfoliated thin sheet of GO is shown in figure 1(b).

As stated in the introduction, the partial reduction of GO can be used to modify the optical properties of the sheets. It was shown that the reduction process is highly sensitive to the amount of reducing agent (hydrazine) [18–20]. A careful tuning of the concentration of hydrazine and the reduction conditions enabled the extraction of the intermediates with particular properties. The fluorescence measurements of the intermediate products of the reduction (supporting information figure S1 (stacks.iop.org/TDM/5/045019/mmedia)) showed that the GO sam-

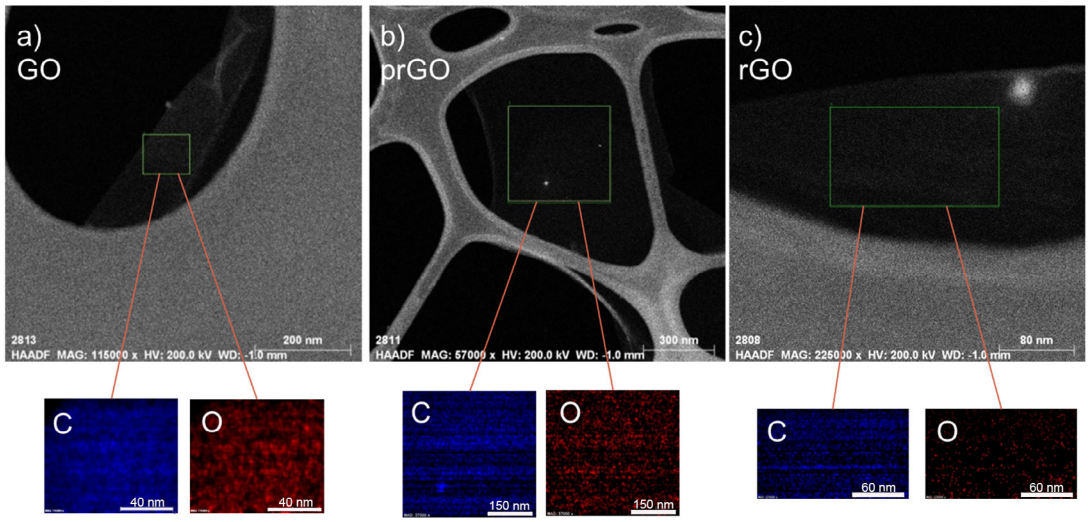

Figure 2. HRTEM micrographs and elemental maps of carbon and oxygen for (a) GO, (b) GO partially reduced for 6 min (prGO) and (c) reduced graphene oxide (rGO). The elemental composition is determined for the selected areas on the sheets surfaces (green outlines).

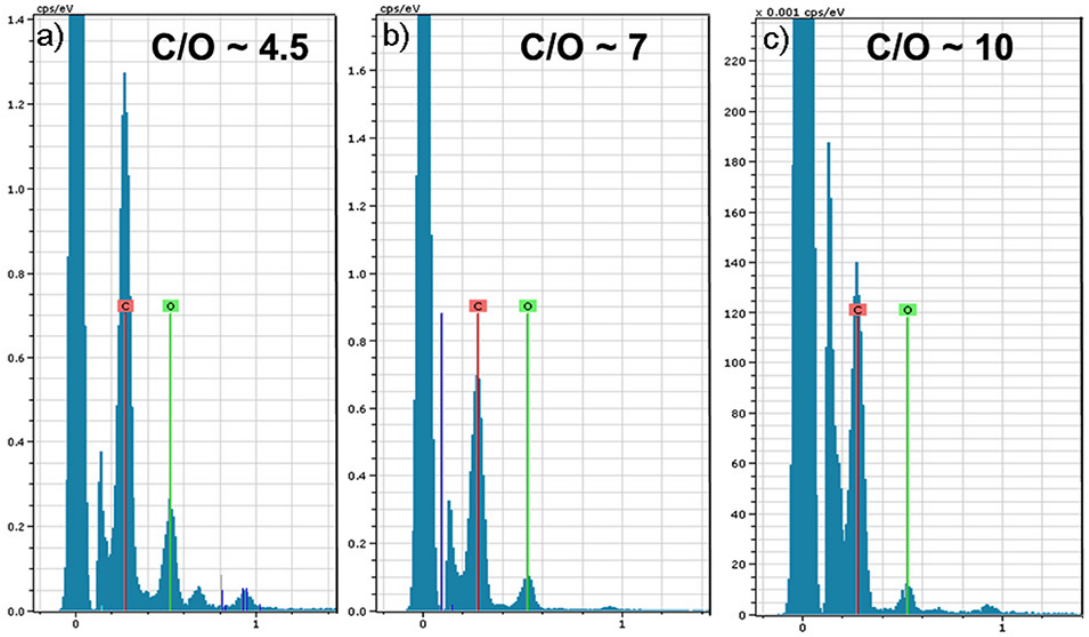

Figure 3. Energy dispersive spectroscopy (EDS) spectra of (a) GO (b) prGO and (c) rGO samples. The ratios of carbon and oxygen atoms increase with increasing in reduction time.

ple partially reduced for 6 min exhibited the highest fluorescence intensity. For this reason, the structural and optical measurements were focused on this particular sample (it will be referred in the text as prGO unless designated otherwise). Figure 2 shows high-resolution TEM micrographs of the initial GO, prGO and rGO samples.

The elemental mappings of the highlighted surface areas are shown under the corresponding TEM images. The oxygen maps (red) reveal that the oxygen content decreases with the time of reduction (figure 2). Thus the C/O ratio is increasing with reduction time, which is also confirmed by EDS results (figure 3). Fabrication of GO led to stable 2 d nanostructures with C/O ~ 4. After the reduction, C/O ratio increased to ~7 for prGO and ~10 for rGO.

The changes in carbon–oxygen ratios were also followed by Raman spectroscopy. Figure 4 shows Raman spectra of the GO, prGO and rGO samples with typical D and G peaks at 1345 cm^{-1} and 1588 cm^{-1} shifts, respectively. The G band originates from the in-plane vibrations of sp^2 carbon atoms and represents doubly degenerate phonon mode (E_{2g} symmetry) at the center of the Brillouin zone. On the other hand, the D peak (A_{1g} symmetry mode) comes from the presence of the sp^3 carbons and from the defect-induced breathing mode of sp^2 rings [21, 22]. Consequently, the reduction process can be followed by observing the changes

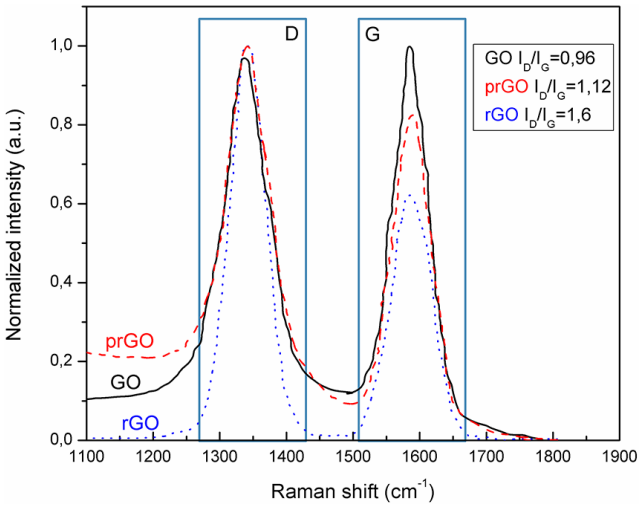

Figure 4. Raman spectra of GO, prGO (GO partially reduced for 6 min) and rGO normalized according to equation (1). The rectangles indicate D and G bands and the ratios of their original intensities are given in the inset.

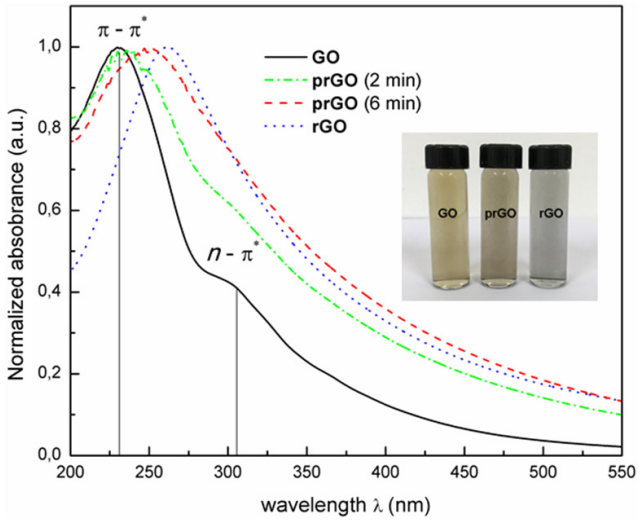

Figure 5. Normalized UV–vis spectra of GO, prGO (partially reduced for 2 and 6 min) and rGO. The inset shows the photo of the obtained GO, prGO (partially reduced for 6 min) and rGO dispersions.

in the relative intensity of these two bands (I_D/I_G). The I_D/I_G ratio of GO is 0.96 and increases after the reduction to 1.12 and 1.60 for prGO and rGO, respectively (figure 4). The reduction affects the in-plane vibrations of sp^2 carbon atoms, which is reflected in changes in the intensity of the G mode (figure 4) [23, 24]. Stankovich *et al* [25] attributed an increase in I_D/I_G ratio to a decrease in the average size of the sp^2 domains upon reduction i.e. to the formation of new graphitic domains that are smaller in size (~2 nm) than those initially present in GO but, at the same time, more numerous in number. The results presented in figure 4 are also in agreement with the Raman spectra reported in the other rGO studies where hydrazine hydrate was used as a reduction agent [26, 27].

The attenuation of light by GO aqueous dispersions during the reduction process was monitored by UV visible spectroscopy (figure 5). The absorption spectra of GO dispersion exhibits two peaks at 220 nm and 310 nm which belong to specified transitions of π–π^* (C = C) and $n - \pi^*$ (C=O), respectively. There is a red shift of the absorbance peak at 220 nm during the reduction. It can also be seen that the shoulder at 310 nm disappeared after the reduction, which is attributed to the decrease in concentration of carboxyl groups [8]. The color of the dispersions also changes during the reduction. The photo of the dispersions is given in the inset of figure 5.

Due to the functionalization (oxidation)-induced opening of the energy gap, GO is expected to exhibit PL. For the excitation in the UV part of the EM spectrum, GO shows pronounced fluorescence emission between 400 and 500 nm, which originates from radiative recombination of electron-hole pairs located in small sp^2 domains [8]. The intensity of the PL emission strongly depends on the time of reduction of GO. It increases with reduction time, reaches the maximum after 6 min and then starts to decrease. The fluorescence

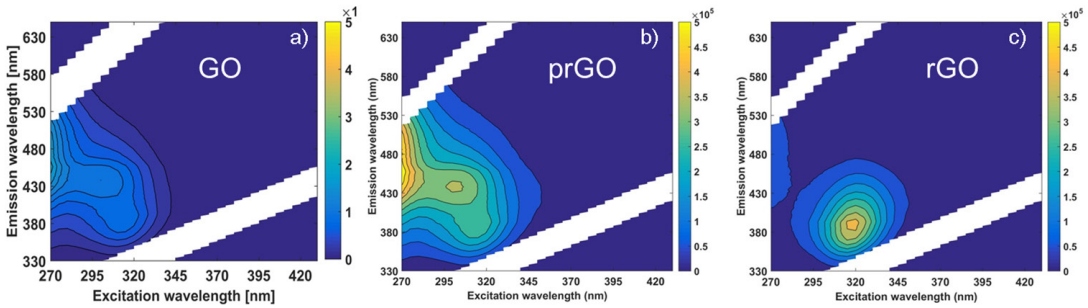

Figure 6. Emission excitation matrices obtained for (a) GO, (b) prGO and (c) rGO samples. The 270–430 nm excitation and 330–650 nm emission wavelength ranges were used.

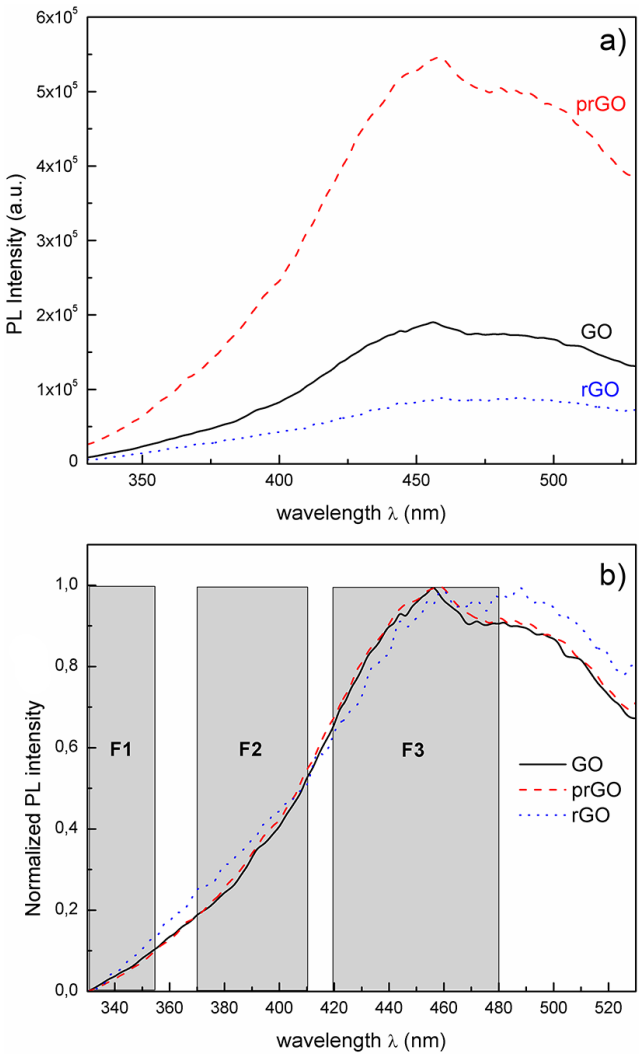

Figure 7. (a) PL emission spectra of GO, prGO and rGO obtained at $\lambda_{exc} = 270$ nm. (b) The same PL spectra normalized with respect to the maximum of the emission intensity. The rectangles indicate the emission ranges F1 [327–353 nm], F2 [370–410 nm] and F3 [420–480 nm] used in deep UV fluorescence imaging.

intensity does not change significantly after prolonged reduction (>10 min). As mentioned above, we will focus on the emission properties of the sample obtained after 6 min of reduction (prGO). PL spectra of the initial GO sample and GO samples reduced at different times are included in Supporting information (figure S1).

The emission excitation matrices of the GO, prGO and rGO are shown in figure 6. As can be seen, there are two distinct regions with pronounced PL intensity noted as region I (λ_{exc} =270 nm, $\Delta\lambda_{em}$ =380–550 nm) and region II (λ_{exc} = 300 nm, $\Delta\lambda_{em}$ = 350–450 nm). Since we intended to study the interaction of GO-based nanosheets with cancer liver cells by DUV

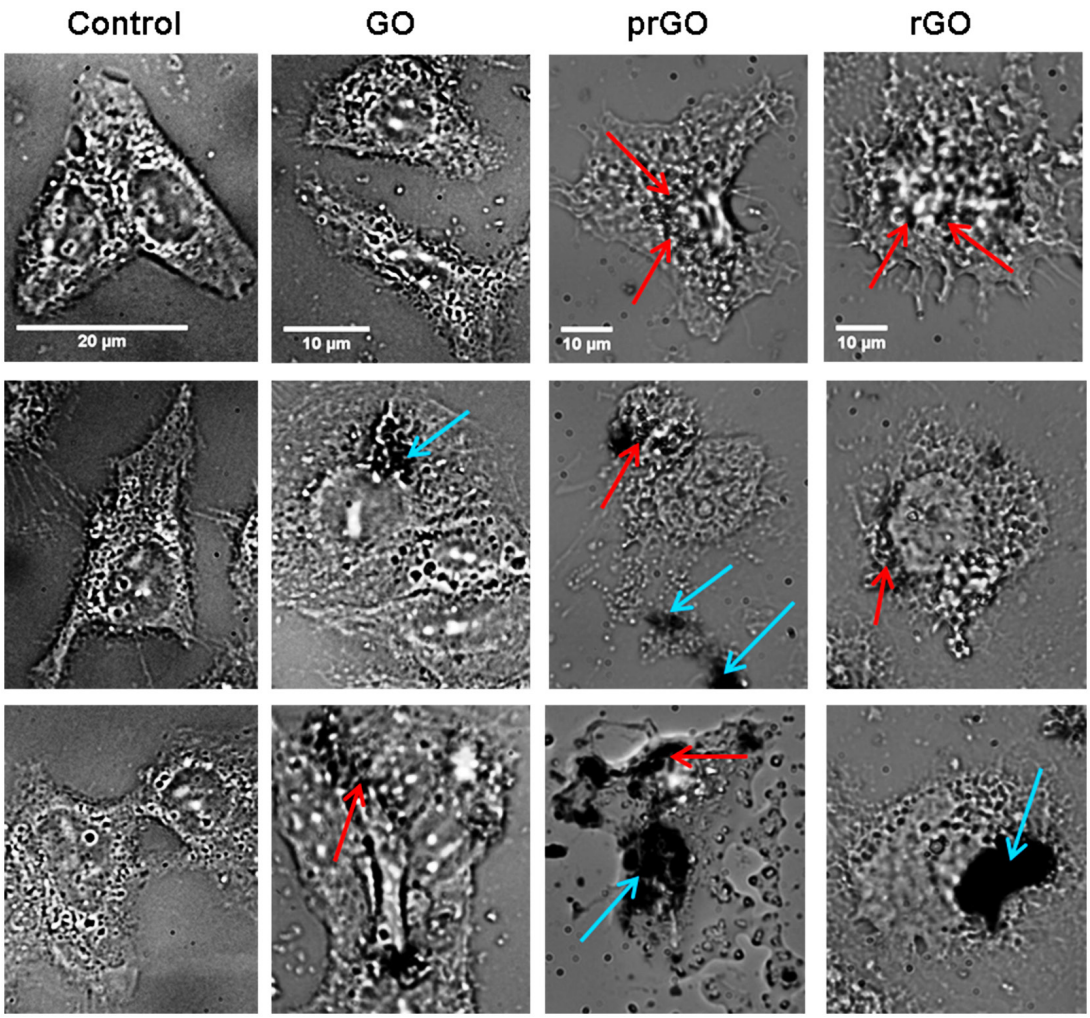

Figure 8. Bright field micrographs of control Huh 7.1.5 cells (1st column) and Huh 7.1.5 cells incubated with GO, prGO and rGO (2nd, 3rd and 4th columns, respectively). Red arrows indicate localization of GO, prGO and rGO at cell sites. Blue arrows indicate non-internalized entities.

imaging, we were interested in the first region with excitation at 270 nm.

Single emission spectra extracted from the emission excitation matrices for $\lambda_{exc} = 270$ nm are shown in figure 7(a).

It can be seen that the prGO yields the highest fluorescence. Apparently, the partial reduction induced specific rearrangement of the honeycomb network which resulted in more effective recombination of excited electrons that further led to the increase in fluorescence intensity. In figure 7(b), we present the normalized PL spectra from figure 7(a). The grey rectangles indicate the emission ranges that are used for the collection of the fluorescence signal in DUV imaging: F1 [327–353 nm], F2 [370–410 nm] and F3 [420–480 nm]. Obviously, the maximum of emission is in F3 range, while all three GO-based species show negligible emission in F1 range.

3.2. DUV Fluorescence imaging of Huh7.5.1 cells incubated with GO, prGO and rGO

Selected visible microscopy images of the control Huh7.5.1 cells and the cells incubated with GO, prGO and rGO are shown in figure 8.

A careful analysis of the cells from various locations along the samples suggested that the morphology of the cells was slightly affected by the presence of GO. GO incubated cancer cells closely resemble the form of the control cells and folded GO aggregates rarely penetrate into the interior of the cells (figure 8, the 1st and 2nd columns). In the case of the cells incubated with prGO and rGO, they are more affected by the presence of the nanosheets and there are nume-rous sites where the sheets are internalized in the cells. It is obvious that degree of the internalization strongly depends on the presence of surface ligands and, consequently, on the reduction level. The agglomerates of internalized reduced graphene oxides are indicated by red arrows (figure 8 the 3rd and 4th columns). This is in agreement with literature data, which showed that cells had the ability to internalize, actively fold and compartmentalize relatively large pieces of the sheets and remain viable [12, 13, 28–30].

Deep UV imaging of treated and untreated Huh7.5.1 cancer liver cells was performed by using the excitation wavelength of 270 nm and the fluorescence emission was monitored in three spectral windows F1 [327–353 nm], F2 [370–410 nm] and F3 [420–480 nm].

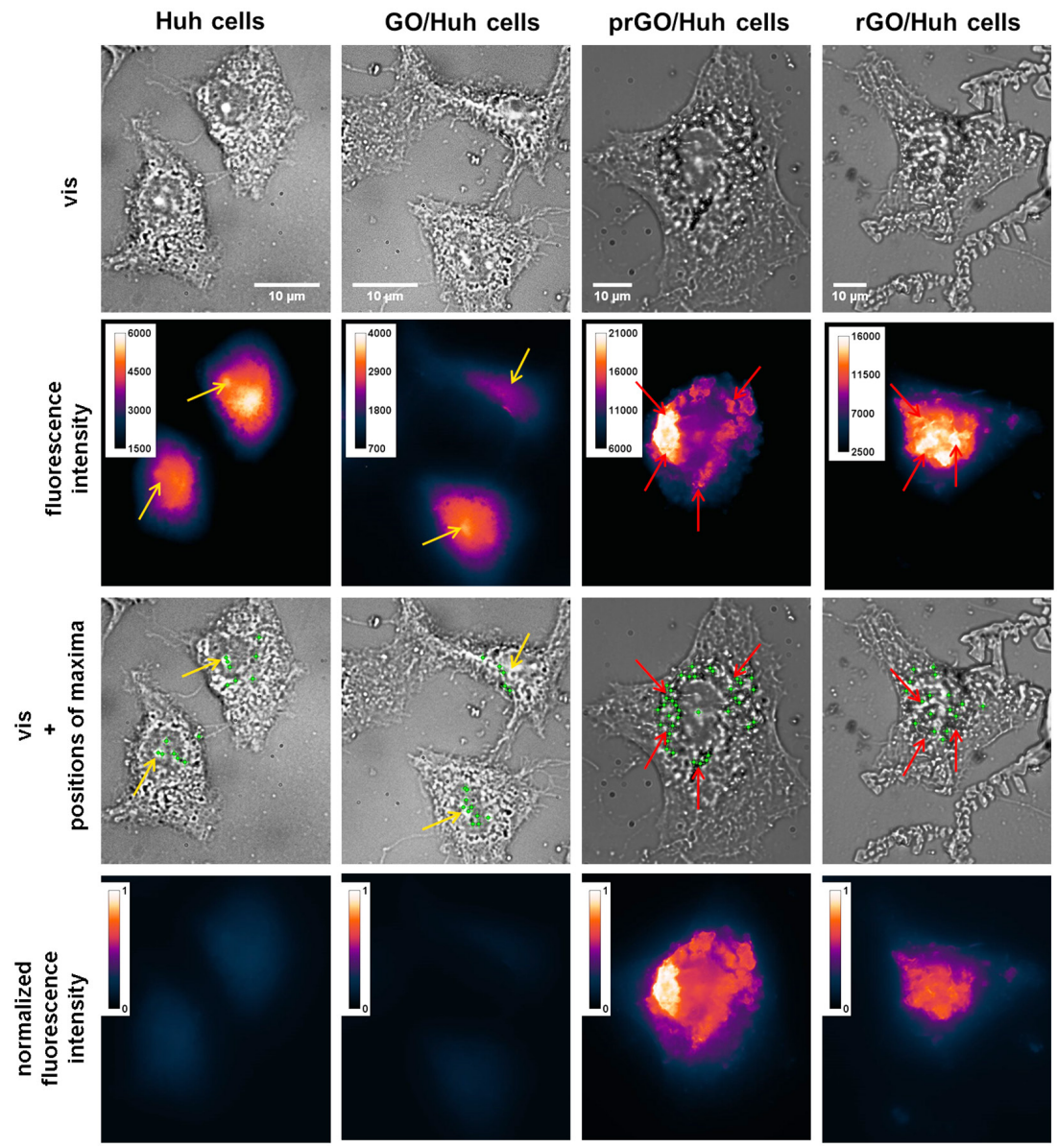

Figure 9. Bright field microscopy (the 1st row) and corresponding DUV fluorescent images (the 2nd row) of the control and GO, prGO and rGO incubated Huh7.5.1 cells in F3 [420–480 nm] emission range. In the 3rd row, the green dots indicate the positions of the local fluorescence maxima (the positions where the intensity of the fluorescence signal exceeds 85% of the maximum fluorescence intensity). The 4th row shows fluorescence images of control and GO, prGO and rGO incubated cells normalized with respect to the maximum intensity obtained for prGO incubated cells.

GO, prGO and rGO fluorescence centers have a wide blue emission that primarily falls into the F3 range (figure 7(b)), and partially into the F2 range. The Huh7.5.1 cells have intrinsic fluorescence that has been detected in all three spectral emission ranges, with comparable fluorescence intensities. Bright field and corresponding fluorescent images of the control and incubated cells in F3 emission range are shown in figure 9. In the second row of figure 9, we show LUT fluorescent images of the cells, while in the fourth row are the same images normalized with respect to the highest intensity observed for the prGO incubated sample for comparison purposes. As can be seen, the fluorescence of GO-incubated is similar to the fluorescence of the control cells (figure 9, the 2nd and 4th row). Also, the fluorescence emission in both samples is mainly homogeneously distributed in the cytoplasmic region. On the other hand, the fluorescence intensities of the prGO/Huh and rGO/Huh samples are much higher than the autofluorescence of the control sample.

Furthermore, it seems that the maxima of the fluorescence coincide with the cell compartments containing internalized prGO and rGO species. In order to show this more clearly, we introduced bright field images with marked positions of the fluorescence maxima (green dots) in the third row of figure 9. To establish the positions of the maxima, the signal intensities were scaled to include the fluorescence that exceeds >85% of the maximum intensity (the details about the scaling procedure and maxima selections can be found in supporting information, figure S2). It is well known that the nucleoli are the brightest intra-

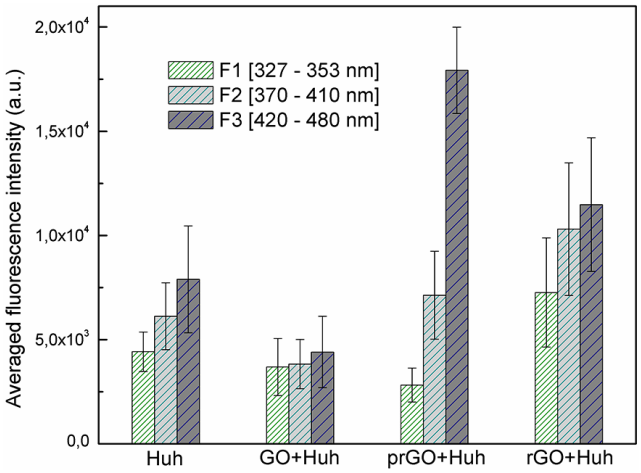

Figure 10. The average fluorescent intensity per single cell for untreated Huh7.5.1 cells (control), as well as GO, prGO and rGO, incubated Huh7.5.1 cells (number of cells counted $n > 30$). The error bars represent standard deviations of the fluorescence intensity.

cellular autofluorescent sites [14, 31] in the nuclei and this is indeed true for the control and GO + Huh samples (the nucleoli are indicated by yellow arrows). In the case of prGO + Huh and rGO + Huh samples, the maxima are positioned on the black entities (indicated by red arrows) suggesting that the fluorescence comes from internalized prGO and rGO. We have selected typical DUV fluorescent images of the control as well as GO, prGO and rGO incubated cells, but the similar fluorescent behavior was noticed at different locations along the sample (the additional images were included in supporting information, figure S3). It is important to notice that the prGO and rGO aggregates localized in the vicinity of the cells do not fluoresce. The lower fluorescence intensity of the prGO (or rGO) aggregates located outside the cell is a consequence of the agglomeration of the sheets. The agglomeration results in the formation of π-stacked complexes, which in turn induces a static quenching [32]. This effect is less pronounced in the case of internalized prGO/rGO because the intracellular material may separate the sheets and prevent the π–π stacking. Further, we calculated the average fluorescent intensities per single cell (number of cells $n > 30$) for all 4 samples, which are presented in figure 10. The results show that the cells with internalized prGO nanostructures have 2.5 times higher fluorescence intensity in F3 range than that of the control samples. It can also be seen that the average fluorescence intensities in all three spectral ranges decrease slightly after incubation with GO. It is possible that GO quenches the main cell fluorophores such as tryptophan, tyrosine, phenylalanine and NADH [33, 34]. Nevertheless, the observed changes are within the experimental error (figure 10). An increase in the fluorescence intensity of Huh7.5.1 cells incubated with rGO, relative to those treated with GO, could be attributed to better internalization of rGO by the cells and consequently reduced π–π stacking. These observations are confirmed by additional DUV fluorescent microscopy measurements on another set of samples. Obviously, the presence of the reduced GO nanostructures affects the overall fluorescence of the Huh7.5.1 cells. We further investigated the fluorescence dynamics with consecutive imaging of the treated and untreated cells.

Selected local fluorescent maxima are followed in the time-lapse experiment (see figure S4 in supporting information for details). The time dependence of the average intensity of local maxima (normalized according to equation (1)) in F1, F2 and F3 emission ranges are shown in figure 11. The original average intensities at particular time intervals and the standard deviations are given in Supporting information (table S1).

It can be seen that the presence of GO based species does not influence the fluorescence kinetics significantly in F1 range. The incubated and control cells show similar time-dependence of the fluorescence intensity (figure 11(a)). The fluorescent intensity decreases with prolonged time, with the slowest decay noticed in the case of the prGO + Huh cells. The time dependence of the fluorescence intensity does not change significantly when the detection was switched from F1 to F2 window (figure 11(b)). The intensity decreases with time in this range as well. However, the degrees of changes are more pronounced. Also, the fastest intensity decay was observed for the GO incubated cells and it should be attributed to the GO-induced emission quenching of tryptophan-containing species mentioned above [33]. In the F3 range (figure 11(c)), the dependence of the fluorescence intensity from time is somewhat different. As can be seen in figure 11(c), the normalized fluorescence intensity of the control cells increases with time. Their fluorescence mostly originates from the presence of NADH, which exhibits maximum fluorescence in this range [15]. Also, the time dependence of the fluorescence intensity of the pure NADH material [35] is similar to that of the control cells observed in figure 11(c).

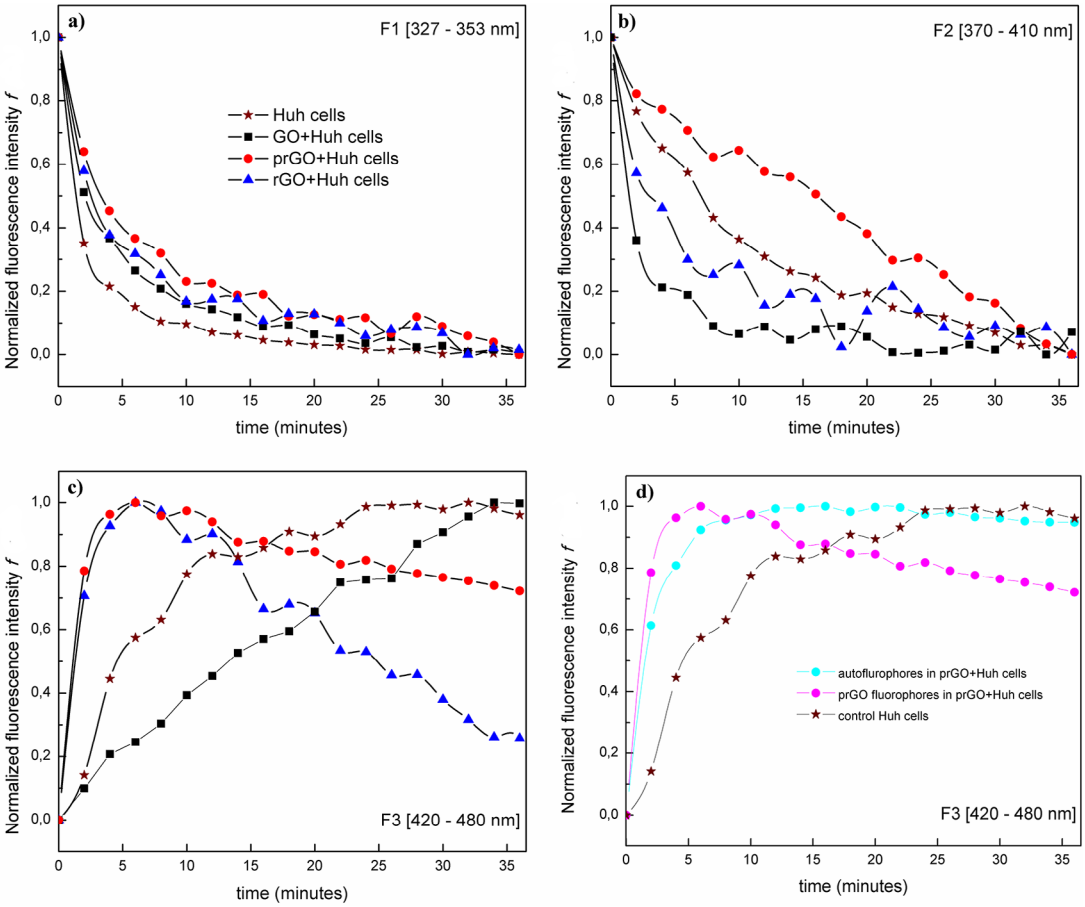

Figure 11. The dependences of the average intensities of local maxima (normalized according to equation (1)) from time in (a) F1 [327–353 nm] (b) F2 [370–410 nm] and (c) F3 [420–480 nm] emission ranges. (d) The evolution of the fluorescent signal that comes from the autofluorophores (fluorescent maxima previously fixed by observing the fluorescence in the F1 range) and from prGO fluorophores in the F3 range (the details about the procedure of finding maxima are explained in the supporting information, figure S5). The curve that corresponds to control Huh cells in (c) is also included in (d) for comparison.

It should also be noticed that the fluorescence of the cells incubated with GO increases almost linearly with time, while the increase itself is slower than that observed for the untreated cells. On the other hand, the reduced graphene oxides (prGO and rGO) affect the fluorescence dynamics differently. The time-lapse experiments show that the fluorescence intensities of prGO and rGO incubated cells reach maxima after approximately 6 min and then start to decrease (figure 11(c)). The obtained results apparently show that GO, prGO and rGO nanosheets affect the fluorescence dynamics in a different way. GO obviously interacts with the cells' autofluorophores, tryptophan (main fluorescence in the F2 range) and NADH (main fluorescence in the F3 range), and induces partial quenching through non-radiative processes. The time-lapse measurements in the F3 range showed the presence of two general processes in the fluorescence of prGO and rGO incubated Huh7.5.1 cells in contrast to the continuous increasing of the fluorescence of the control cells. In figure 11(d), we tried to follow the time dependence of the fluorescence intensities of the autofluorophore (NADH) and fluorophore prGO in the prGO incubated cells separately. The details of the procedure are explained in the supporting information (figure S5). Briefly, the positions of the fluorescence maxima in F1 range (which correspond almost exclusively to the fluorescence of the autofluorophores) were fixed. After that, the time evolution of these fluorescence centers was followed in the F3 range together with the time evolution of strongest fluorescence centers in the same range (which coincide with the positions of prGO sheets). As the results in figure 11(d) show, the fluorescence dynamics of the autofluorophores in the F3 range closely resembles the dynamics of control cells in the same range. The fluorescence intensity is increasing with time until it reaches saturation. This suggests that the change in fluorescence dynamics of prGO + Huh cells with respect to that of the control cells is indeed the consequence of the presence of prGO fluorophores. A deeper understanding of the effects of prGO on the time evolution of fluorescent signal would require a separate study. Nevertheless, the presented results (figures 9 and 10) clearly show that the average fluorescence intensity of the cells significantly increases if they are incubated with prGO sample. Since it contains both sp^2 and sp^3 domains, it may interact with aromatic ring containing drugs through π–π stacking but also with polar molecules via epoxide, hydroxyl, and carboxylic groups. This is why

we believe that prGO can also be used in drug delivery applications. The successful delivery of the drug conjugated to prGO nanosheets might be monitored by fluorescence imaging and we plan to continue our research in this direction.

4. Conclusion

In this article, DUV fluorescence spectroscopy was used to study the interaction of prGO with the cancer liver cells. A modified Hummers method was used for the fabrication of GO and the reduction was performed in the presence of hydrazine hydrate. The partial reduction of GO was achieved by controlling the duration of the reduction process. It was found that the sample partially reduced for 6 min showed the highest fluorescence intensity and it was further used in bioimaging tests. GO, prGO and rGO samples were studied using various microscopy and spectroscopic methods in order to establish their structure and physical properties. STEM micrographs of GO, prGO and rGO showed the presence of isolated monolayers. Elemental analysis revealed that the C/O ratio values were dependent on the time of reduction, which was also confirmed by Raman spectroscopy. The change in the optical properties was monitored by PL and UV–vis spectroscopies. The prGO showed the highest intensity of PL emission for the excitation that belongs to the DUV part of the EM spectrum. The fluorescent GO, prGO and rGO nanostructures were used in the DUV fluorescence imaging study of the cancer liver cell line Huh7.5.1. The interaction of the prGO nanostructures with the cells resulted in a strong increase in the fluorescence intensity in F3 [420–480 nm] range with respect to the autofluorescence of the control sample. Time-lapse studies showed that the time dependence of the fluorescence emission from GO, prGO and rGO internalized cells is different from that of the intrinsic fluorescence of the untreated cells. The prGO nanostructure was suggested as a possible carrier for cancer drugs since its pronounced fluorescence might be used for monitoring the delivery process. In the forthcoming study, we will focus on the drug conjugated-prGO nanostructures and their interaction with cancer cells.

Acknowledgments

Deep UV imaging was performed at the DISCO beamline of Synchrotron SOLEIL (France). This study was financially supported by Ministry of Education and Science and Technological Development, Republic of Serbia (Project Nos. 172056, 45020 and 171029) and projects NSF CREST (HRD-0833184) and NASA (NNX09AV07A).

ORCID iDs

Dušan K Božanić https://orcid.org/0000-0001-8246-9635
Miroslav Dramićanin https://orcid.org/0000-0003-4750-5359
Vladimir Djoković https://orcid.org/0000-0001-8237-1101

References

[1] Cheng C, Li S, Thomas A, Kotov N A and Haag R 2017 Functional graphene nanomaterials based architectures: biointeractions, fabrications, and emerging biological applications *Chem. Rev.* **117** 1826–914
[2] Du D, Yang Y and Lin Y 2012 Graphene-based materials for biosensing and bioimaging *MRS Bull.* **37** 1290–6
[3] Mahanta S and Paul S 2015 Bovine α-lactalbumin functionalized graphene oxide nano-sheet exhibits enhanced biocompatibility: a rational strategy for graphene-based targeted cancer therapy *Colloids Surf.* B **134** 178–87
[4] Zhang S, Yang K, Feng L and Liu Z 2011 *In vitro* and *in vivo* behaviors of dextran functionalized graphene *Carbon* **49** 4040–9
[5] Lu C, Huang P-J J, Liu B, Ying Y and Liu J 2016 Comparison of graphene oxide and reduced graphene oxide for DNA adsorption and sensing *Langmuir* **32** 10776–83
[6] Lu C, Huang P-J J, Liu B, Ying Y and Liu J 2013 Exploring the origin of blue and ultraviolet fluorescence in graphene oxide *J. Phys. Chem. Lett.* **4** 2035–40
[7] Demchenko A P and Dekaliuk M O 2013 Novel fluorescent carbonic nanomaterials for sensing and imaging *Methods Appl. Fluoresc.* **1** 042001
[8] Eda G, Lin Y-Y, Mattevi C, Yamaguchi H, Chen H-A, Chen I-S, Chen C-W and Chhowalla M 2010 Blue photoluminescence from chemically derived graphene oxide *Adv. Mater.* **22** 505–9
[9] Xin G, Meng Y, Ma Y, Ho D, Kim N, Cho S M and Chae H 2012 Tunable photoluminescence of graphene oxide from near-ultraviolet to blue *Mater. Lett.* **74** 71–3
[10] Chien C-T *et al* 2012 Tunable photoluminescence from graphene oxide, *Angew. Chem., Int. Ed.* **51** 6662–6
[11] Morimoto N, Kubo T and Nishima Y 2016 Tailoring the oxygen content of graphite and reduced graphene oxide for specific applications *Sci. Rep.* **6** 21715
[12] Chatterjee N, Eom H J and Choi J 2014 A systems toxicology approach to the surface functionality control of graphene-cell interactions *Biomaterials* **35** 1109–27
[13] Corr S J, Raoof M, Cisneros B T, Kuznetsov O, Massey K, Kaluarachchi W D, Cheney M A, Billups E W, Wilson L J and Curley S A 2013 Cytotoxicity and variant cellular internalization behavior of water-soluble sulfonated nanographene sheets in liver cancer cells *Nanoscale Res. Lett.* **8** 208
[14] Monici M 2005 Cell and tissue autofluorescence research and diagnostic applications *Biotechnol. Annu. Rev.* **11** 227–56
[15] Heikal A A 2010 Intracellular coenzymes as natural biomarkers for metabolic activities and mitochondrial anomalies *Biomark. Med.* **4** 241–63
[16] Galande C, Mohite A D, Naumov A V, Gao W, Ci L, Ajayan A, Gao H, Srivastava A, Bruce Weisman R and Ajayan P M 2011 Quasi-molecular fluorescence from graphene oxide *Sci. Rep.* **1** 85
[17] Schindelin J *et al* 2012 Fiji: an open-source platform for biological-image analysis *Nat. Methods* **9** 676
[18] Gao X, Jang J and Nagase S 2010 Hydrazine and thermal reduction of graphene oxide: reaction mechanisms, product structures, and reaction design *J. Phys. Chem.* C **114** 832
[19] Chua C K and Pumera M 2015 The reduction of graphene oxide with hydrazine: elucidating its reductive capability based on a reaction-model approach *Chem. Commun.* **52** 72–5
[20] Chua C K and Pumera M 2014 Chemical reduction of graphene oxide: a synthetic chemistry viewpoint *Chem. Soc. Rev.* **43** 291–312
[21] Ferrari C and Robertson J 2000 Interpretation of Raman spectra of disordered and amorphous carbon *Phys. Rev.* B **61** 14095–107

[22] Tuinstra F and Koenig J L 1970 Raman spectrum of graphite *J. Chem. Phys.* **53** 1126–30
[23] Yang D *et al* 2009 Chemical analysis of graphene oxide films after heat and chemical treatments by x-ray photoelectron and micro-Raman spectroscopy *Carbon* **47** 145–52
[24] Yin F, Wu S, Wang Y, Wu L, Yuan P and Wang X 2016 Self-assembly of mildly reduced graphene oxide monolayer for enhanced Raman scattering *J. Solid State Chem.* **237** 57–63
[25] Stankovich S, Dikin D A, Piner R D, Kohlhaas K A, Kleinhammes A, Jia Y, Wu Y, Nguyen S T and Ruoff R S 2007 Synthesis of graphene-based nanosheets via chemical reduction of exfoliated graphite oxide *Carbon* **45** 1558–65
[26] Tung V C, Allen M J, Yang Y and Kaner R B 2009 High-throughput solution processing of large-scale graphene *Nat. Nanotechnol.* **4** 25–9
[27] Paredes J I, Villar-Rodil S, Solis-Fernandez P, Martinez-Alonso A and Tascon J M D 2009 Atomic force and scanning tunneling microscopy imaging of graphene nanosheets derived from graphite oxide *Langmuir* **25** 5957–68
[28] Lammel T, Boisseaux P, Fernandez-Cruz M L and Navas J M 2013 Internalization and cytotoxicity of graphene oxide and carboxyl graphene nanoplatelets in the human hepatocellular carcinoma cell line Hep G2 *Part. Fibre Toxicol.* **10** 27
[29] Shin S R *et al* 2014 Layer-by-layer assembly of 3D tissue constructs with functionalized graphene *Adv. Funct. Mater.* **24** 6136–44
[30] Park J *et al* 2015 Graphene oxide flakes as a cellular adhesive: prevention of reactive oxygen species mediated death of implanted cells for cardiac repair *ACS Nano* **9** 4987–99
[31] Konig K K, So P T C, Matulin W W, Tromberg B J and Gratton E 1996 Two photon excited lifetime imaging of autofluorescence in cells UVA and NIR photostress *J. Microsc.* **183** 197–204
[32] Kim J, Kim F and Huang J 2010 Seeing graphene-based sheets *Mater. Today* **13** 28–38
[33] Li S, Aphale A N, Macwan I G, Patra P K, Gonzalez W G, Mikovska J and Leblanc R M 2012 Graphene oxide as a quencher for fluorescent assay of amino acids, peptides, and proteins *ACS Appl. Mater. Interfaces* **4** 7069–75
[34] Zhao Y, Hsieh H-S, Wang M and Jafvert C T 2017 Light-independent redox reactions of graphene oxide in water: electron transfer from NADH through graphene oxide to molecular oxygen, producing reactive oxygen species *Carbon* **123** 216–22
[35] Zhao Y, Hsieh H-S, Wang M and Jafvert C T 2004 NADH enzyme-dependent fluorescence recovery after photobleaching (ED-FRAP): applications to enzyme and mitochondrial reaction kinetics, *in vitro Biophys. J.* **86** 629–45